Chiral Heterometallic Ag_4Cu_4 Nanocluster: Environment-Sensitive Phosphorescence and Efficient Electrocatalytic Nitrate Reduction to Ammonia

Jiafan Ou, [a] [b] Yan Nong, [a] Zhixun Zhang, [a] [b] Hualing Yang, [c] Xianyong Yu,*[a] Huayan Yang*[b]

[a] Key Laboratory of Theoretical Organic Chemistry and Functional Molecules, Hunan University of Science and Technology, Xiangtan, Hunan, China

E-mail: Huayan Yang: yanghuayan@fjirsm.ac.cn; yu_xianyong@163.com

[b] State Key Laboratory of Structural Chemistry, Fujian Institute of Research on the Structure of Matter, Chinese Academy of Sciences, Fuzhou, Fujian 350002, P. R. China

[c] School of Chemistry and Chemical Engineering, Nantong University, Nantong, Jiangsu, China

Experiment Section

Chemicals and Materials.

N-Phenyl-o-phenylenediamine, KOH, CS_2, anhydrous Na_2SO_4, $AgNO_3$, tetraethylammonium copper(I) tetrafluoroborate, absolute ethanol, triethylamine, methanol, acetonitrile, dichloromethane (CH_2Cl_2), n-hexane and ethyl acetate were used as received. Deuterated chloroform ($CDCl_3$, 99.8%D, containing 0.03% TMS) was purchased from Beijing Bailingwei Technology Co., Ltd. A perfluorinated resin dispersion (analytical grade, 20 wt%) was obtained from Shanghai Titan Scientific Co., Ltd. K_2SO_4, KNO_3, NaOH, potassium sodium tartrate tetrahydrate, sodium hypochlorite solution (available chlorine ≥ 5.2%) and sodium nitroprusside (sodium nitroferricyanide) were used as received. All solvents were of analytical grade, and deionised water was used throughout.

Synthesis of 1-phenyl-1,3-dihydro-2H-benzo[d]imidazole-2-thione

The synthesis was performed according to a reported procedure with minor modifications. *N*-Phenyl-*o*-phenylenediamine (4.0 g, 21.17 mmol) was dissolved in absolute ethanol (220 mL) in a 500 mL round-bottom flask under stirring. An aqueous solution of KOH (3.647 g, 65.13 mmol) in H_2O (87 mL) was added, followed by dropwise addition of CS_2 (3.9 mL, 65.13 mmol). The reaction mixture was fitted with a reflux condenser and heated to reflux in an oil bath at 70 °C for 14 h. After cooling to room temperature, the mixture was concentrated under reduced pressure to remove most of the solvents. The residue was transferred to a separatory funnel and extracted with CH_2Cl_2 (60 mL) and H_2O (120 mL). The aqueous phase was further extracted with CH_2Cl_2 (2 × 30 mL). The combined organic layers were dried over anhydrous Na_2SO_4, filtered, and concentrated in vacuo to afford the crude product. The crude solid was dissolved in a minimal amount of CH_2Cl_2, and *n*-hexane was slowly added under sonication until complete precipitation occurred. The precipitate was collected by filtration and washed with pre-cooled CH_2Cl_2. The resulting solid was dried under vacuum at 60 °C for 24 h to give a white powder (2.4 g, 52% yield).^{1}H NMR (500 MHz, $CDCl_3$) δ

7.70–7.49 (m, 5H), 7.31 (d, *J* = 7.88 Hz, 1H), 7.22 (td, *J* = 7.73, 1.13 Hz, 1H), 7.15 (td, *J* = 7.71, 1.16 Hz, 1H), 6.97 (d, *J* = 7.87 Hz, 1H).

Synthesis of [$Ag_4Cu_4(C_{13}H_9N_2S)_8$]

$AgNO_3$ (20 mg, 0.118 mmol) and tetraethylammonium copper(I) tetrafluoroborate (25 mg, 0.079 mmol) were charged into a 20 mL glass vial and dissolved in MeCN (8 mL). A solution of 1-phenyl-1,3-dihydro-2H-benzo[d]imidazole-2-thione (30 mg, 0.13 mmol) in CH_2Cl_2 (8 mL) was then added, followed by triethylamine (50 μL) and MeOH (4 mL). The vial was sealed, sonicated for 30 min to ensure thorough mixing, and heated at 70 °C for 24 h in an oven. Upon completion, yellow crystals formed at the bottom of the vial. The vial was left standing at room temperature for 2 d to allow slow solvent evaporation. The crystals were collected by filtration and washed with EtOAc to remove uncoordinated ligand, affording [$Ag_4Cu_4(C_{13}H_9N_2S)_8$] as yellow crystals (26.8 mg, 54% yield based on Cu). Elemental analysis calcd (%) for $C_{104}H_{72}Ag_4Cu_4N_{16}S_8$: C 50.21, H 2.92, N 9.01; found: C 50.82, H 2.39, N 9.16.^{1}H NMR (400 MHz, DMSO-d6) δ 7.99 – 6.90 (m, 8H), 6.80 (d, *J* = 8.0 Hz, 1H).

CCDC 2508177.

Apparatus and Characterization

D8 VENTURE X-ray single crystal diffractometer (Bruker, Germany), Rigaku SmartLab powder X-ray diffractometer (Rigaku, Japan), AVANCE NEO 500 MHz superconducting NMR spectrometer (Bruker, Switzerland), UV-2600i UV-visible spectrophotometer (Shimadzu, Japan), Fluorescence Spectrometer (Fluorolog-QM), Electrochemical Workstation (CHI 760E, Shanghai Chenhua Instruments Co.), Mass Spectrometer (Waters SYNAPT XS), Steady-State and Transient Fluorescence Spectrometer (Edinburgh FLS1000), Elemental Analyzer (Elementar vario EL cube).

Single-crystal X-ray diffraction. Single-crystal X-ray diffraction data for [$Ag_4Cu_4(C_{13}H_9N_2S)_8$] were collected at 100 K on a Bruker D8 VENTURE diffractometer equipped with a Cu Kα radiation source (λ = 1.54178 Å). The structure was solved using SHELXT within the Olex2 program suite and refined by full-matrix least-squares on F^2 using SHELXL.

Powder X-ray diffraction (PXRD). PXRD patterns of the bulk samples were recorded at room temperature on a Rigaku SmartLab diffractometer equipped with a Cu Kα radiation source (λ = 1.54178 Å) operating at 40 kV and 40 mA. The data were collected in the 2θ range of 5° to 50° with a scan rate of 5° min^{-1}.

Photophysical measurements. Photoluminescence measurements were performed under vacuum. The absolute photoluminescence quantum yield (PLQY) was determined using an integrating sphere. Time-resolved photoluminescence (TRPL) lifetimes were recorded under the same conditions, and variable-temperature solid-state emission spectra were collected in vacuo.

Preparation of working electrodes. Carbon paper (1 × 1 cm²) was used as the working electrode, and the catalyst was loaded by a drop-casting method. The catalyst loading was fixed at 0.5 mg cm^{-2}. To prepare the catalyst ink, catalyst powder (1.5 mg) was dispersed in a mixed solvent (300 μL) consisting of ethanol and Nafion solution (v/v = 49:1), followed by ultrasonication for 30 min to afford a homogeneous suspension. The resulting ink was then drop-cast onto the carbon paper and dried at ambient conditions prior to electrochemical measurements.

Electrochemical measurements. The electrochemical nitrate reduction (NO_3^-RR) was investigated in an H-type two-compartment cell using 0.5 M K_2SO_4 as the electrolyte, where the cathodic and anodic chambers were separated by an FAA-3-50 ion-exchange membrane. Electrochemical measurements were carried out on a CHI 760E electrochemical workstation (CH Instruments, Shanghai, China) using a standard three-electrode configuration. A catalyst-loaded carbon paper electrode (1 × 1 cm²) served as the working electrode, a Pt electrode as the counter electrode, and an Ag/AgCl electrode as the reference electrode. The working electrode was placed in the cathodic chamber and positioned at a fixed distance from the reference electrode. Both chambers were filled with 30 mL of 0.5 M K_2SO_4. All potentials were converted to the reversible hydrogen electrode (RHE) scale using the Nernst equation.

$$\mathbf{E_{RHE} = E_{Ag/AgCl} + 0.1976 + 0.0591 \times pH \ (pH = 7)}$$

Linear sweep voltammetry (LSV) was performed in 30 mL of an aqueous electrolyte containing 0.5 M K_2SO_4 and 0.1 M KNO_3, over the potential range of +0.2 to −1.4 V (vs. RHE) at a scan rate of 5 mV s^{-1}. Electrochemical impedance spectroscopy (EIS) was conducted at −0.9 V (vs. RHE) with an AC amplitude of 10 mV over the frequency range of 0.1 Hz to 100 kHz. The EIS data were fitted using an equivalent circuit to extract the charge-transfer resistance (*R*ct) associated with the NO_3^- reduction process.

NH_3 quantification and Faradaic efficiency

Faradaic efficiency (FE_{NH3}) was calculated as:

$$FE_{NH3} = \frac{n\ V_{electrolyle}\ C_{NH3}\ F}{Q}$$

where n=8 is the number of electrons required to produce 1 mol of NH3 from NO_3^-, F is the Faraday constant (96485 C mol^{-1}), C_{NH_3} is the molar concentration of NH3 in the catholyte, V is the catholyte volume (0.030 L), and Q is the total charge passed during electrolysis.

The NH3 yield rate was calculated as:

$$YR_{NH3} = \frac{n_{NH3}}{g_{cat.}\,t}$$

where n_{NH_3} is the amount (mol) of NH_3 produced, g_{cat} is the mass of catalyst loaded on the electrode, and t is the electrolysis time.

NH_3 was quantified by the indophenol blue method: The liquid products collected after continuous electrolysis for 60 min were diluted with deionised water to ensure that the NH_3 concentration fell within the linear range of the indophenol assay. The colour reagent was prepared by dissolving salicylic acid (0.036 mol), potassium sodium tartrate tetrahydrate (0.018 mol) and NaOH (0.036 mol) in deionised water (100 mL). For the colorimetric analysis, 4 mL of the diluted sample was mixed with 500 µL of the colour reagent, 50 µL of 0.034 M sodium nitroprusside solution ($C_5FeN_6Na_2O$), 50 µL of NaClO solution (6–14% available chlorine), and 0.75 M NaOH solution. The mixture was allowed to stand for ~1 h until full colour development. UV–Vis absorption spectra were then recorded, and the NH_3 concentration was determined from the absorbance at ~674 nm.

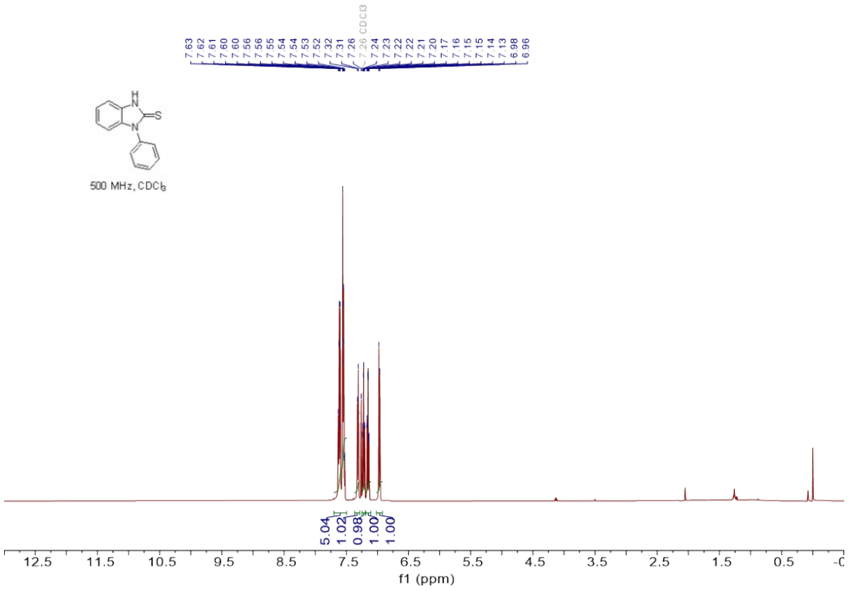

Figure S1. ^{1}H NMR spectrum of 1-phenyl-1,3-dihydro-2H-benzo[d]imidazole-2-thione (*500 MHz, $CDCl_3$, 298 K*).

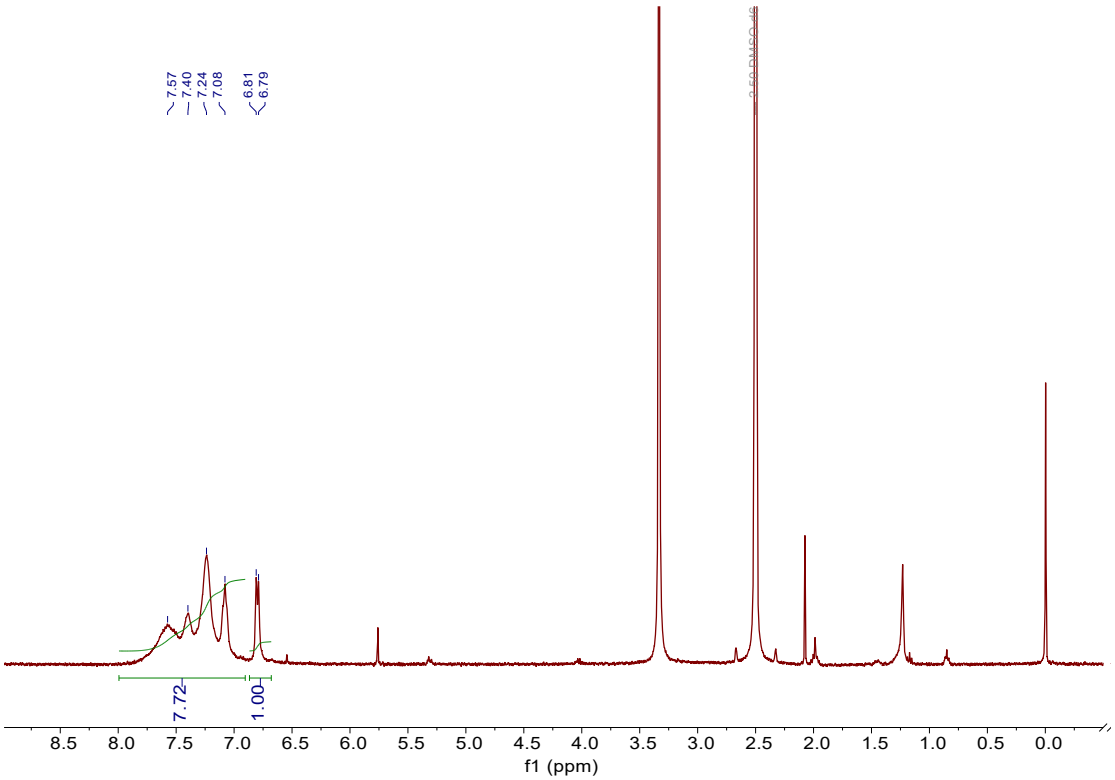

Figure S2. ^{1}H NMR spectrum (400 MHz, DMSO-d6, 298 K) of the Ag_4Cu_4 nanocluster. The broad multiplet signals in the aromatic region (6.8–8.5 ppm) confirm the successful coordination of the 1-phenyl-1,3-dihydro-2H-benzo[d]imidazole-2-thione ligands onto the cluster core. This significant peak broadening, compared to the free ligand, is caused by the restricted rotation of the phenyl rings within the dense ligand layer and intra-molecular π-π stacking interactions on the cluster surface (consistent with the supramolecular lock and RIM mechanisms). Furthermore, the sharp signals in the aliphatic region (< 5.0 ppm) are assigned to trace amounts of residual solvents from the post-synthetic washing and crystallization processes, rather than impurities: ethyl acetate (1.17 ppm (t), 1.99 ppm (s), 4.03 ppm (q)) and n-hexane (0.88 ppm, 1.26 ppm). The solvent residual peak of DMSO and the water peak are observed at 2.50 ppm and ~3.33 ppm, respectively.

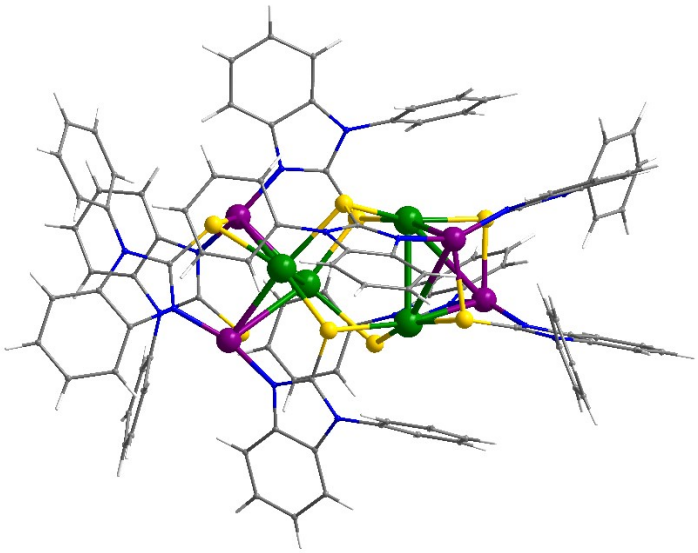

Figure S3. The structure of $[Ag_4Cu_4(C_{13}H_9N_2S)_8]$. Ag, Cu, S, N, C and H atoms are represented by green, purple, yellow, blue, grey and white spheres, respectively.

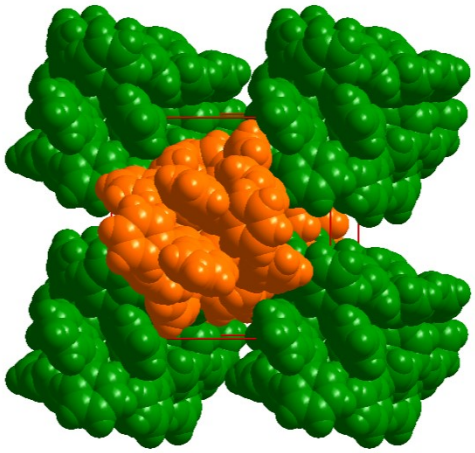

Figure S4. The packing structure of $[Ag_4Cu_4(C_{13}H_9N_2S)_8]$ of the unit cell, which is recamic. Two enantiomers are highlighted in different colors.

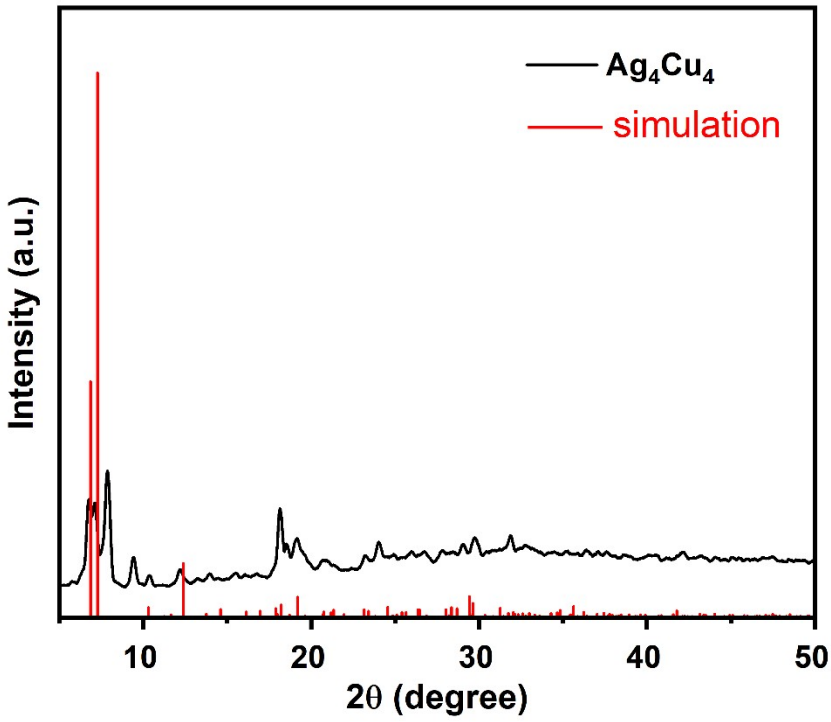

Figure S5. Powder X-ray diffraction (PXRD) patterns of the Ag4Cu4 nanocluster. The black line represents the experimental data of the bulk sample at room temperature, and the red bars denote the simulated pattern derived from the single-crystal X-ray diffraction data. The experimental pattern acceptably matches the main diffraction peaks of the simulated one (particularly the characteristic low-angle peaks around 2θ = 7–10°), confirming the high phase purity and retained crystallinity of the synthesized bulk sample.

Fit Results

Fit: $A+B1\exp(-t/\tau_1)$

Decay Scan	: **Decay1 on Em1**
File location	: File has not been saved.
Range (ch)	: 0 to 1999
Peak Count	: 75 in channel 4
Total Count	: 35534
Time Calibration	: 50.000 ns/ch
Total Experiment Time	: 880.00 s
Fit Range (ch)	: 5 to 1999

Parameter	Value	Std. Dev.	Rel %
τ_1	1.627E-005 s	1.662E-007 s	
B1	89.2423	0.8443	100.00
A	2.0363		
χ^2	1.1924		

Figure S6. Representative time-resolved photoluminescence (TRPL) decay profile and mono-exponential fitting results for $[Ag_4Cu_4(C_{13}H_9N_2S)_8]$ in the solid state under vacuum. The decay was fitted with $I(t) = A + B_1 exp(-t/\tau_1)$, giving $\tau_1 = 1.63 \times 10^{-5}$ s (16.3 μs) with $\chi^2 = 1.19$.

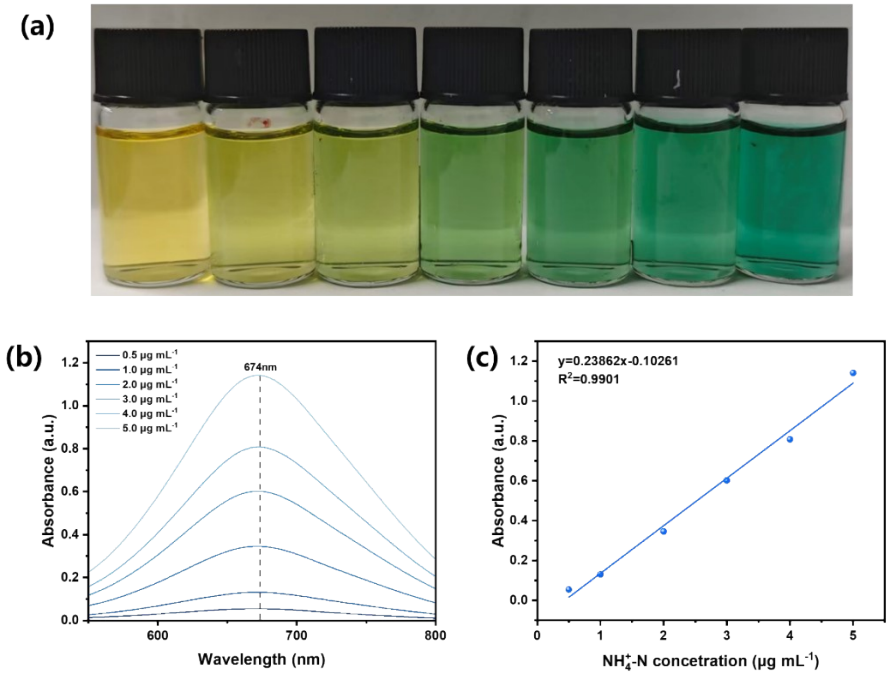

Figure S7. (a) Photographs of indophenol blue solutions prepared with different NH_4^+ concentrations for NH_3 quantification; (b) UV–Vis absorption spectra of NH_4^+ standards after 1 h incubation in the indophenol blue assay; (c) Calibration curve for NH_3 constructed using

NH_4Cl standard solutions in ultrapure water.

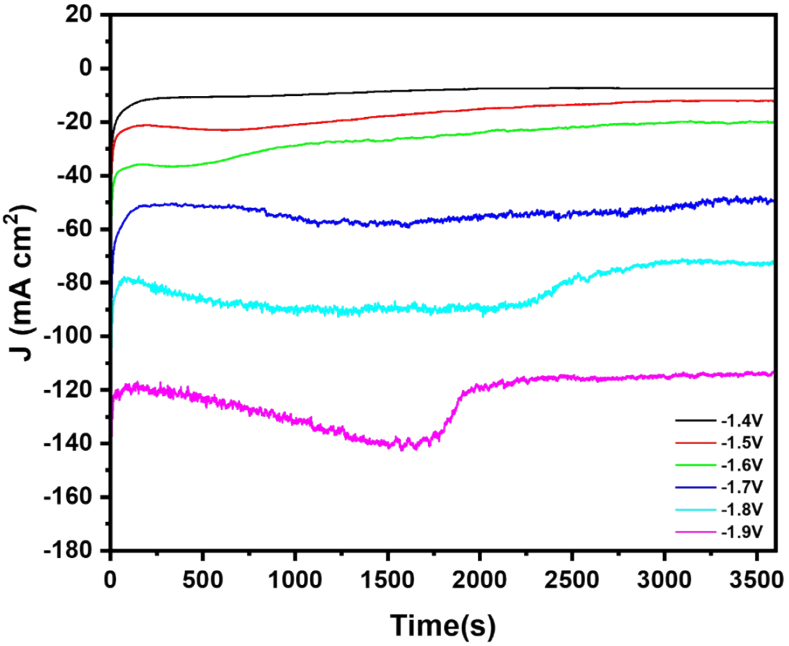

Figure S8 Chronoamperometric i–t curves of the Ag_4Cu_4 cluster for electrocatalytic NH_3 synthesis recorded at different applied potentials.

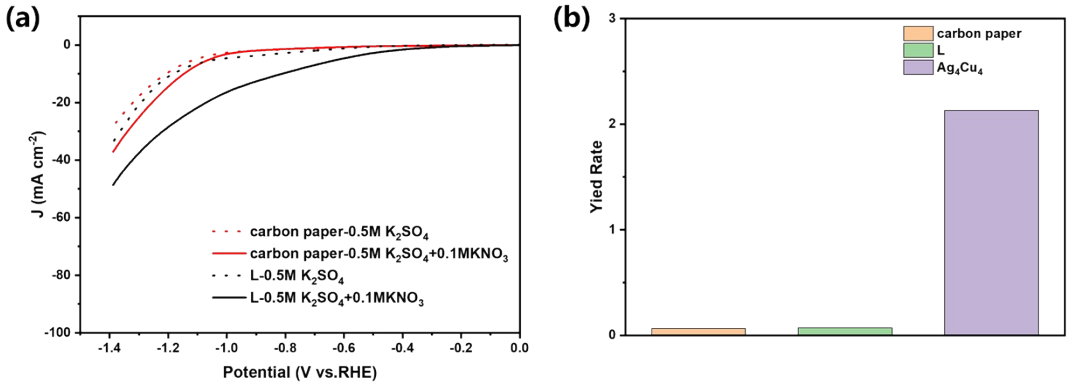

Figure S9 Control experiments. (a) LSV curves of the catalyst-free electrode (carbon paper coated with an identical Nafion binder film) and the ligand-only electrode recorded in 0.5 M K_2SO_4 with/without 0.1 M KNO_3. (b) NH_3 yield after potentiostatic electrolysis at –0.89 V vs RHE under identical conditions. Trace NH_3 was detected for both the catalyst-free and ligand-only electrodes only in the presence of KNO_3, while no NH_3 was detected in nitrate-free electrolyte. The Ag_4Cu_4 electrode exhibited a substantially higher NH_3 yield than either control.

Table S1 Crystallographic data and structure refinement parameters for $[Ag_4Cu_4(C_{13}H_9N_2S)_8]$.

Empirical formula	$C_{104}H_{72}Ag_4Cu_4N_{16}S_8$
Formula weight	2488.022
Temperature/K	100.00
Crystal system	tetragonal
Space group	$P\bar{4}2_1C$
a/Å	17.1574(5)
b/Å	17.1574(5)
c/Å	19.4626(8)
α/°	90
β/°	90
γ/°	90
Volume/Å^3	5729.3(3)
Z	2
ρ_{calc}g/cm^3	1.442
μ/mm^{-1}	7.912
F(000)	2477.8
Crystal size/mm^3	0.006 × 0.006 × 0.004
Radiation	Cu Kα (λ = 1.54178)
2Θ range for data collection/°	6.86 to 136.72
Index ranges	$-16 \le h \le 20$, $-18 \le k \le 15$, $-23 \le l \le 23$
Reflections collected	25757
Independent reflections	5218 [R_{int} = 0.0804, R_{sigma} = 0.0687]
Data/restraints/parameters	5218/0/307
Goodness-of-fit on F^2	1.028
Final R indexes [I>=2σ (I)]	R_1 = 0.0437, wR_2 = 0.0994
Final R indexes [all data]	R_1 = 0.0582, wR_2 = 0.1061
Largest diff. peak/hole / e Å^{-3}	0.92/-0.67
Flack parameter	0.020(7)

Table S2 Comparison of representative cluster-based electrocatalysts for electrochemical nitrate reduction to ammonia

Catalyst	Catalyst type	Electrolyte	Working condition	FE for NH_3 (%)	NH_3 yield rate	Ref.
$Au_{28}Cu_{12}$	Atomically precise bimetallic nanocluster	Ar-saturated 0.05 M H_2SO_4 + 0.5 M KNO_3	−0.7 V vs RHE (max FE); −1.0 V vs RHE (max yield)	97	6.54 $mg \cdot metal^{-1} \cdot h^{-1}$	1
$Ag_{20}Cu_{12}$	Atomically precise bimetallic nanocluster	0.5 M Na_2SO_4 containing 500 ppm NO_3^-	−0.5 to −0.9 V vs RHE	84.6	2.34 $mg \cdot h^{-1} \cdot mg^{-1}$	2
DNA-templated Cu nanoclusters (CuNCs)	Cu nanoclusters	1 M KOH + 0.1 M NO_3^-	−0.6 V vs RHE	96.8	2.62 $mg \cdot h^{-1} \cdot cm^{-2}$	3
$Cu_4(PTI)_4$	Atomically precise Cu_4 cluster	0.5 M K_2SO_4 + 0.1 M KNO_3	−40 mA cm^{-2}	~100	2.66 $mg \cdot h^{-1} \cdot mg^{-1}$	4
$Cu_4(BTT)_4$	Atomically precise Cu_4 cluster	0.5 M K_2SO_4 + 0.1 M KNO_3	−40 mA cm^{-2}	~75	N.R.	4
$Ag_4Cu_4(L)_8$	Atomically precise chiral heterometallic nanocluster	0.5 M K_2SO_4 + 0.1 M KNO_3	−0.89 V vs RHE	78.9	2.13 $mg \cdot h^{-1} \cdot cm^{-2}$	This work

Note: NH_3 yield rates are reported using the original normalization basis in the cited literature (per metal mass, catalyst mass, or geometric area), and are therefore not forcibly converted to a single unit.

References

1. S. Tang, T. Song, X. Cai, W. Ding and Y. Zhu, Chem. Commun., 2024, 60, 7785–7788.

2. G. Ma, F. Sun, L. Qiao, Q. Shen, L. Wang, Q. Tang and Z. Tang, Nano Res., 2023, 16, 10867–10872.

3. W. Luo, S. Wu, Y. Jiang, P. Xu, J. Zou, J. Qian, X. Zhou, Y. Ge, H. Nie and Z. Yang, ACS Appl. Mater. Interfaces, 2023, 15, 18928–18939.

4. H. Chen, K.-S. Qi, X.-Y. Dong, Y.-N. Pei, Y.-J. Jin, H. Zhang, S. Li, J. Wu, J. Cai and S.-Q. Zang, Angew. Chem. Int. Ed., 2025, 64, e202510429